Hindawi Publishing Corporation
Advances in Materials Science and Engineering
Volume 2009, Article ID 601850, 9 pages
doi:10.1155/2009/601850

Research Article

Fabrication of Highly Porous Alumina-Based Ceramics with Connected Spaces by Employing PMMA Microspheres as a Template

Kazutaka Kamitani,[1] Takeo Hyodo,[1] Yasuhiro Shimizu,[2] and Makoto Egashira[2]

[1] *Graduate School of Science and Technology, Nagasaki University, 1-14 Bunkyo-machi, Nagasaki 852-8521, Japan*
[2] *Department of Materials Science and Engineering, Faculty of Engineering, Nagasaki University, 1-14 Bunkyo-machi, Nagasaki 852-8521, Japan*

Correspondence should be addressed to Yasuhiro Shimizu, shimizu@nagasaki-u.ac.jp

Received 18 May 2009; Revised 29 July 2009; Accepted 25 November 2009

Recommended by Krystyn J. Van Vliet

Highly porous alumina-based ceramics were fabricated by a slip casting method by employing polymethylmethacrylate (PMMA) microspheres having different diameters as a template and MgO or SiC powder as a sintering aid and subsequent calcination at 1600°C. Spherical pores reflecting the morphology of the PMMA microspheres could be fabricated. In addition, the formation of much smaller connected space among the pores was observed on the pore's inner walls of all ceramics. In this method, porous structure, for example, pore diameter, shape (open or closed), and mechanical properties, could be controlled by varying the particle size of PMMA microspheres and its concentration in alumina-based slurries. Highly porous and mechanically strong alumina-based ceramics having an open porosity of 62%, a connected space size of 1.3 μm, and a compressive strength of 147.6 MPa could be fabricated by employing PMMA microspheres with a mean particle size of 22.6 μm and an appropriate amount of SiC.

1. Introduction

There are currently widespread interests in porous ceramics owing to their specific properties, such as low bulk density, low specific heat, low thermal conductivity and high specific surface area. Among them, permeability of various gaseous and liquid substances through porous ceramics, which can be improved drastically by controlling the open porosity strictly, is one of interesting properties, because porous ceramics with well-developed open pores have been applied in wide technological fields such as filters for molten metals, catalyst carriers, insulators at high temperatures, lightweight structural materials, biomaterials and so on [1–7]. Generally, these properties are largely dependent on the kind of pore-forming procedures [8, 9], such as a polymeric sponge replication [10, 11], direct foaming [12–14], template method [15, 16] and sol-gel method [17]. However, it is extremely difficult to achieve large open porosity as well as high mechanical strength of porous ceramics even by using any methods as described above. For example, Tian et al. have succeeded in preparing well-developed porous ceramics (pore size: 200 ~ 500 μm and open porosity: 70% ~ 82%) by a sol-gel method with a polymeric sponge replication [18]. However, their porous ceramics showed only low mechanical properties (compressive strength: less than 3.0 MPa). We have also prepared various porous materials such as hollow ceramic microspheres with a diameter of several tens microns and porous films with sub-micron sized spherical pores by utilizing a mehcanofusion system [19] and a modified sol-gel technique by employing polymethylmethacrylate (PMMA) microspheres as a template [19–23], respectively. For example Kato et al. demonstrated that the compressive strength of the hollow alumina microsphere prepared by utilizing the mechanofusion system was much higher than commercial ones and the hollow alumina was very promising as an additive to Al metal-based composites for weight-saving

Table 1: Compositions of slurries used for slip-casting.

Sample	Al_2O_3 (g)	PMMA microsphere Mean particle size (μm)	PMMA microsphere g	MgO (g)	SiC (g)	SiO_2 (g)	Water (mL)	Theoretical porosity (%)
P20NONE	15	22.6	10	0	0	0	7.0	68.9
P60NONE		62.2					7.2	68.9
P90NONE		96.7					7.5	68.9
P20MgO(1)		22.6		0.1			7.5	68.7
P20MgO(3)		22.6		0.3			8.5	68.5
P60MgO(1)		62.2		0.1			8.0	68.7
P90MgO(1)		96.7					8.5	68.7
P20SiC(1)		22.6		0	0.1		7.0	68.8
P20SiC(3)		22.6			0.3		7.0	68.4
P20SiO_2(4.5)		22.6		0	0	0.45	7.5	67.8

200 μl polyvinyl alcohol, 200 μl polycarboxylic acid ammonium, and 0.1 g polyethylene glycol were added to each slurry.

[24]. In addition, the porous films prepared by the modified sol-gel technique showed excellent sensing properties to H_2, NO_x, H_2S and inflammable gases [20–23, 25], because of the modified gas reactivity and diffusivity. Some porous materials such as microspheres and thin films supported by a dense substrate could be prepared easily by the above preparation techniques, but it is also very difficult to prepare porous bulk bodies having both large open porosity and high mechanical strength, which are indispensable in the fields of filters, catalyst supports and biomaterials. On the other hand, it is well-known that a slip-casting method is very suitable for preparing ceramic bulk bodies with large volume and various porous bulk bodies have already been fabricated by the addition of various pore-formers in their raw slurries [26–28]. For example, Albano et al. have succeeded in preparing porous ceramics (mean pore size: ca. 9 μm) by a slip-casting method employing the spherical granule of starch (mean particle size: 10 μm) and acrylic latex (mean particle size: 0.37 μm) [28]. However, the open porosity of the resultant ceramics was relatively low (ca. 54.7%), due to the formation of a limited numbers of connected spaces in the green bodies. In addition, they have not achieved high mechanical strength yet, owing to the poor distribution and morphology of pores and the partly destructed ceramic skeletons. Thus, further drastic improvement in both the open porosity and the mechanical strength of porous bulk ceramics is of primary importance in various application fields presently.

In this study, therefore, attempts were made to establish the preparation conditions of porous alumina-based ceramics with well-developed and well-controlled PMMA-originated pores with connected spaces as well as sufficient mechanical strength by the slip-casting method employing PMMA microspheres as a template, followed by firing at elevated temperatures. Connected spaces between PMMA-originated pores were developed from direct contact points or shrinkage of very thin walls of alumina-based ceramics among PMMA microspheres during the sintering. Effects of SiC and MgO additives on the porous structure and mechanical properties of the resulting porous alumina-based ceramics have also been tested.

2. Experimental Procedure

2.1. Preparation of Porous Ceramics. A basic alumina slurry was prepared by the following procedure: 15 g of high purity alumina powder (TM-DAR: Taimei Chem. Co., Ltd.) with an average particle size of 0.1 μm and 10 g of spherical cross-linked PMMA microspheres with a mean particle size of 22.6 μm (MR-20G, Soken Chem. & Eng. Co., Ltd.) as a pore former were mixed with 7.0 mL of deionized water. In addition, 200 μl of polyvinyl alcohol (Wako Pure Chem. Indus., Ltd.) as a binder, 200 μl of polycarboxylic acid ammonium (Toagosei Co., Ltd.) as a deflocculation agent and 0.1 g of polyethylene glycols (Wako Pure Chem. Indus., Ltd.) as an antifoaming agent were added to the mixture, and then the resultant mixture was subjected to ball milling at a rotation speed of 400 rpm for 30 minutes to make an uniform slurry. Other PMMA microspheres purchased from Soken Chem. & Eng. Co., Ltd., MR-60G (ca. 62.2 μm in diameter) and MR-90G (ca. 96.7 μm in diameter), were also used as a pore former to prepare other kinds of slurries as listed in Table 1. The maximum open porosity of 74%, which is calculated by assuming the complete occupation of dense alumina in the opening among closely packed PMMA microspheres (as a hard-sphere) with a uniform diameter, may be achieved by carefully adjusting the experimental conditions. In the present study, however, the experimental conditions were set to achieve the maximum open porosity in the range of 67% and 69% theoretically, by referring to our preliminary experiments. The slurry obtained is expressed as P*m*NONE compacts, where P represents the addition of PMMA, *m* stands for the kind of PMMA added (i.e., $m = 20$ means the use of MR-20G), and NONE means the addition of no sintering aid. Other kinds of slurries containing different amounts of MgO (Kyowa Chem. Indus. Co., Ltd.), SiC (OY-15, Yakushima Denko Co., Ltd.) or SiO_2 (Kishida Chem. Co., Ltd.) as a sintering aid were also prepared in a similar manner. Detailed compositions of these slurries and then their abbreviations are also summarized in Table 1. Namely, as for P20SA(*n*) compacts, the meanings of P and 20 have already been explained as

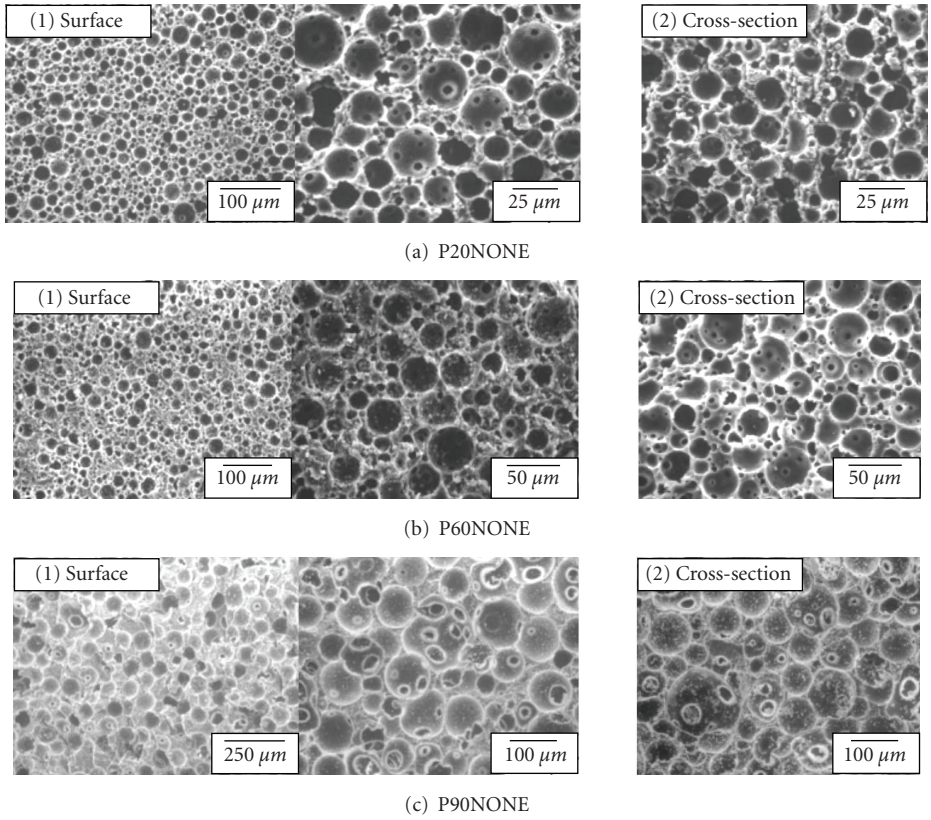

Figure 1: SEM photographs of (a) P20NONE, (b) P60NONE, and (c) P90NONE.

above, SA represents the kind of the sintering aid used, that is, MgO or SiC, and (n) means the ten times of an additive amount of the sintering, respectively. During the sintering of compacts in air, SiC is expected to oxidized to SiO_2, therefore, SiO_2 is also tested another kind of sintering aid and the SiO_2 additive amount was controlled to be the same amount of SiO_2 formed from the added SiC. Taking into accounts of the densities of alumina, sintering aids and PMMA, these compositions were designed so as to achieve a theoretical porosity of 68.9% of resulting ceramics after the thermal decomposition of PMMA, that is, removal of PMMA. These slurries were poured into a glass pipe (inside diameter: 5 mm, hight: 15 mm) on a plaster board, then were dried at 45°C for 24 hours, while the top of glass pipe was covered by a glass plate. Therefore, the solvent of these slurries was absorbed to the plaster downward. PMMA and other organic additives were eliminated from the slip cast compacts by thermal decomposition by heating at a heating rate of $0.5^\circ C\,min^{-1}$ up to 450°C and folding at the same temperature for 0.5 hour in air. Thereafter the compacts were heated at a heating rate of $10^\circ C\,min^{-1}$ up to 1600°C and were sintered at the same temperature for 2 hours. The resulting porous alumina-based ceramic compact is also referred to as the same abbreviation as that of the slurry used for fabricating the compact. For the measurement of compressive strengths, porous alumina-based ceramics were processed into circular cylinder bars with approximately 4.4 mm in diameter and 10 mm thick by polishing.

2.2. Characterization. Microstructure of porous alumina-based ceramics fabricated was observed by scanning electron microscope (SEM, Hitachi High-Technologies Corp., S-2250N). The average diameter of PMMA microspheres and PMMA-originated pores was determined by measuring diameters of about a number of 800 of PMMA microspheres and PMMA-originated pores each in their SEM photographs, respectively. In addition, the mean diameter of connected spaces was determined by measuring diameters of a number of 1000 connected spaces in their SEM photographs.

Pore size distributions of porous alumina-based ceramics were measured by a mercury porosimeter (Micromeritics Instrument Corp., AutoPore IV 9500). The open porosity was calculated by using the pore volume measured by the mercury porosimeter and the true density measured by a multivolume pycnometer (Micromeritics Instrument Corp., 1305). The crystal phase was characterized by X-ray diffraction (XRD, Rigaku Corp., RINT-2200) using CuKα radiation (30 kV, 16 mA). Compressive strength was measured with a universal testing machine (Shimadzu Corp., Autograph AGS-5kND) at a crosshead speed of $0.1\,mm\,min^{-1}$. The cross-sectional area of the processed ceramics and the maximum mechanical failing load were used to calculate the compressive strength. The average value of ten samples for each porous alumina-based ceramic was used to evaluate the effects of the size of PMMA microspheres and the amount of sintering aids on the mechanical strength of the porous alumina-based ceramics.

Table 2: Microstructural and mechanical properties of porous alumina-based ceramics.

Samples	SEM photograph		Hg porosimeter			XRD	Compressive strength (MPa)
	Average diameter (μm)		Pore volume ($cm^3\ g^{-1}$)	Pore diameter (μm)	Experimental open porosity (%)	Crystallite size (nm)	
	PMMA-originated pore	Connected spaces					
P20NONE	20.8	3.5	0.35	2.1	58	20.9	95.8
P60NONE	58.2	7.2	0.34	7.0	57	22.1	49.5
P90NONE	89.3	13.6	0.34	11.6	57	22.8	28.7
P20MgO(1)	20.2	2.5	0.28	1.8	52	30.5	125.4
P20MgO(3)	18.8	1.8	0.27	1.6	51	34.5	138.5
P60MgO(1)	56.7	6.2	0.27	6.5	51	32.4	57.4
P90MgO(1)	87.7	12.3	0.26	10.8	50	33.2	32.8
P20SiC(1)	20.1	1.9	0.41	1.6	62	42.8	128.5
P20SiC(3)	19.4	1.6	0.41	1.3	62	60.4	147.6
P20SiO_2(4.5)	19.5	1.8	0.36	1.6	58	57.4	125.2

3. Result and Discussion

3.1. Morphology and Characteristics of Porous Alumina-Based Ceramics

3.1.1. Effect of Mean Particle Sizes of PMMA Microspheres on Microstructure of PmNONE Compacts. Figure 1 shows SEM photographs of three kinds of P*m*NONE compacts. From these photographs, formation of spherical pores was confirmed at both the surface and the cross-section of all P*m*NONE compacts. The diameter of these pores formed was not uniform and varied in a certain range, but reflected well the shape of original PMMA microspheres used as a template. Thus, these pores can be referred to as PMMA-originated pores. Table 2 summarizes microstructural and mechanical properties of P*m*NONE compacts fabricated in the present study. As described in the experimental procedure, the mean particle sizes of PMMA microspheres used are 22.6 μm for MR-20G, 62.2 μm for MR-60G and 96.7 μm for MR-90G, respectively. However, average diameters of PMMA-originated pores are 20.8 μm for P20NONE compact, 58.2 μm for P60NONE compact and 89.3 μm for P90NONE compact, respectively. Thus, a shrinkage of ca. 10% in diameter was observed, irrespective of the different sizes of PMMA microspheres used, in the case of porous alumina-based ceramics without any sintering aids. In addition, the formation of connected spaces among the PMMA-originated pores was observed on their inner walls in all P*m*NONE compacts. Such connected spaces are considered to be developed from direct contact points or very thin layers of alumina particles among PMMA microspheres in the dried compacts by the shrinkage during the sintering. From the SEM photographs, the average diameter of the connected space was measured to be 3.5 μm for P20NONE compact, 7.2 μm for P60NONE compact and 13.6 μm for P90NONE compact. Thus, it was revealed that the diameter of connected spaces could be controlled by the size of the PMMA microspheres used as a template. Figure 2 shows pore size distributions of P*m*NONE compacts. Although almost the same total pore volume was measured with all P*m*NONE compacts (see Table 2), the pore diameter at the maximum pore volume increased with an increase in the mean particle size of PMMA microspheres used; 2.1 μm for P20NONE compact, 7.0 μm for P60NONE compact, 11.6 μm for P90NONE compact. By considering the measurement principle of the mercury porosimeter, the pores measured can be regarded as the narrowest and/or bottleneck pores, that is, the diameter of the connected spaces among the PMMA-originated pores as shown in Figure 1. Actually, the pore diameter at the maximum pore volume is well coincident with the average diameter of connected spaces of P*m*NONE compacts. As explained in the experimental section, theoretical porosity of all samples was controlled to be 68.9%, but the open porosity, which was calculated from the pore volume and the true density, of P*m*NONE compacts were slightly smaller than the theoretical porosity, as summarized in Table 2. This may arise from a certain grain growth among α-Al_2O_3 crystallites even if no sintering aid is added. Figure 3(a) shows an XRD pattern of P20NONE compact. The crystallite sizes of α-Al_2O_3 in all P*m*NONE compacts, which was calculated by using Scherrer's equation, are summarized in Table 2. The diffraction peaks ascribed only to an α-Al_2O_3 phase were observed for P20NONE compact, but the crystallite size of α-Al_2O_3 became almost doubled (20.9 nm), as compared with that of the starting material, α-Al_2O_3 powder (ca. 9.5 nm). In addition, it was revealed that the size of PMMA microspheres used seems to have little effect on the grain growth of α-Al_2O_3.

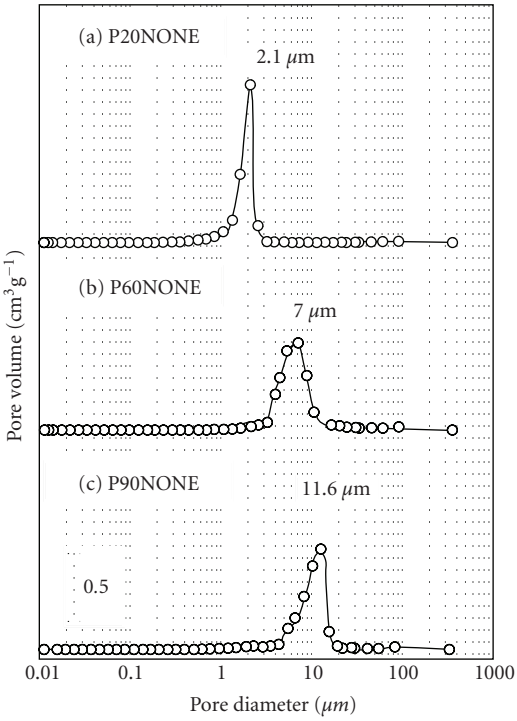

Figure 2: Pore size distributions of (a) P20NONE, (b) P60NONE, and (c) P90NONE.

3.1.2. Effect of the Kind of Sintering Aids on Microstructure of PmSA(n) Compacts. Figures 3(b) and 3(c) show XRD patterns of P20MgO(3) and P20SiC(3) compacts, respectively, and crystallite sizes of α-Al_2O_3 in several P20SA(n) compacts are summarized in Table 2. As for P20MgO(3) compact, large diffraction peaks of α-Al_2O_3 were observed along with unknown small ones, and the crystallite size of α-Al_2O_3 (34.5 nm) was larger than that of P20NONE compact. On the other hand, no additional peaks except for α-Al_2O_3 were obvious in the case of P20SiC(3) compact, but the crystallite size (60.4 nm) increased drastically in comparison with that of P20MgO(3). To get the information on impurities formed in P20SA(3) compacts, α-Al_2O_3 powder mixed with an equivalent amount of MgO or SiC powder was calcined at 1600°C for 2 hours in air. XRD patterns of the resulting powders, which were denoted as 50 wt% MgO-Al_2O_3 and 50 wt% SiC-Al_2O_3, respectively, are shown in Figures 3(d) and 3(e), respectively. As for 50 wt% MgO-Al_2O_3, $MgAl_2O_4$ was observed as a main phase, while a small amount of MgO was also detected. Thus, the additional small peaks other than α-Al_2O_3 observed in Figure 3 (b) can be ascribed to $MgAl_2O_4$. On the other hand, $Al_6Si_2O_{12}$ was confirmed as a main phase of 50 wt% SiC-Al_2O_3, but its formation was not confirmed in the case of P20SiC(3) compact (Figure 3(c)). However, P20SiC(3) compact showed very sharp peaks of α-Al_2O_3 and the narrow half value of width in comparison with P20NONE compact. This implies that SiC-related compounds dissolve in α-Al_2O_3 and then promotes effectively the grain growth of the α-Al_2O_3 crystallites.

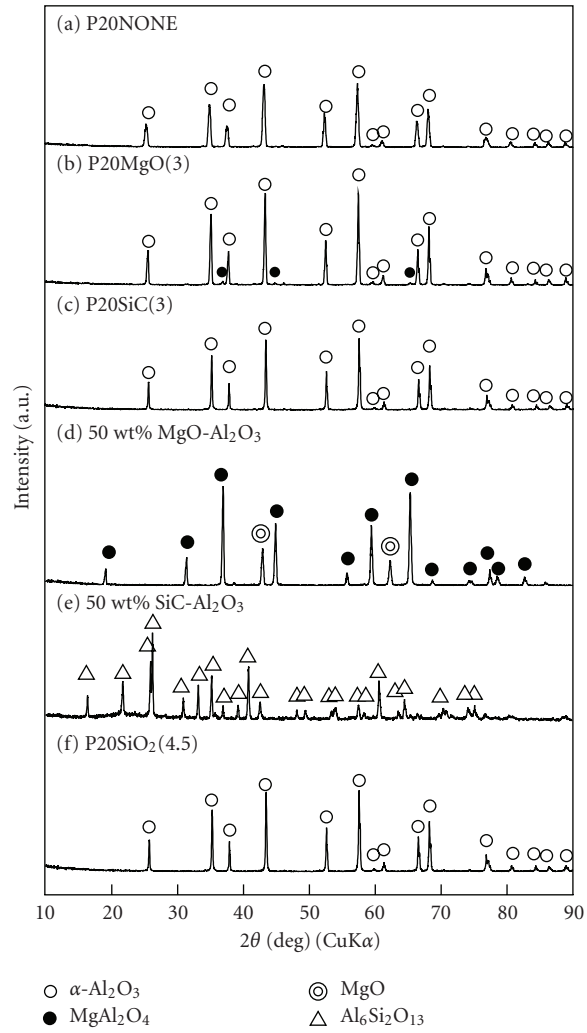

Figure 3: XRD patterns of (a) P20NONE, (b) P20MgO(3), (c) P20SiC(3), (d) 50 wt% MgO-Al_2O_3, (e) 50 wt% SiC-Al_2O_3 and (f) P20SiO_2(4.5).

The effect of the diameter of PMMA microspheres on the microstructural morphology of PmMgO(1) compacts was also investigated. But a similar tendency as that for PmNONE compacts was observed, as summarized in Table 2. Namely, the diameters of both the PMMA-originated pores and the connected spaces increased gradually with an increase in diameter of PMMA microspheres as a template, while the pore volume and the crystallite size remained almost unchanged.

The effect of the amounts of MgO addition on the microstructural morphology was also examined in the series of P20MgO(n) compacts. Figures 4 and 5 show SEM photographs and pore size distributions of representative P20MgO(n) compacts. Microstructural morphology of P20MgO(1) compact was similar to that of P20NONE compact (see Figure 1(a)), but the average diameters of both the PMMA-originated pores and the connected spaces in P20MgO(1) compact were slightly smaller than those

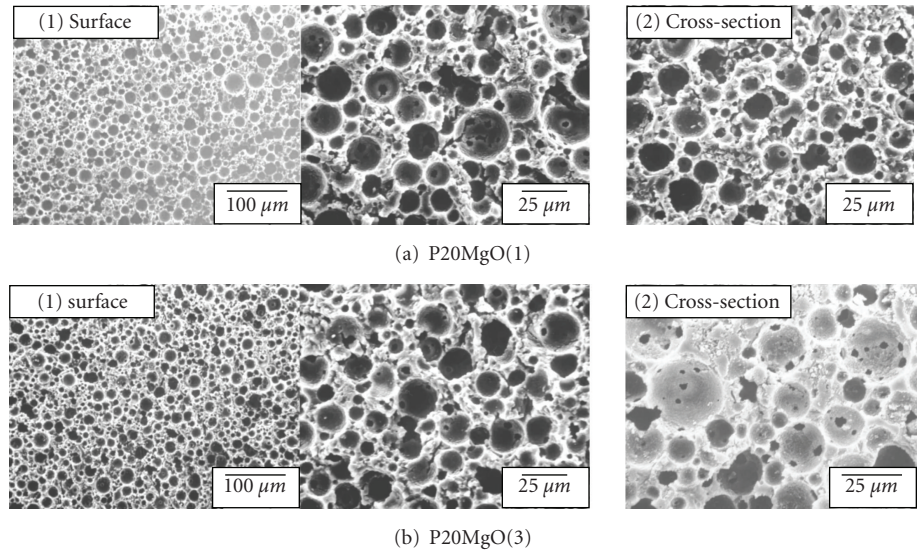

Figure 4: SEM photographs of (a) P20MgO(1) and (b) P20MgO(3).

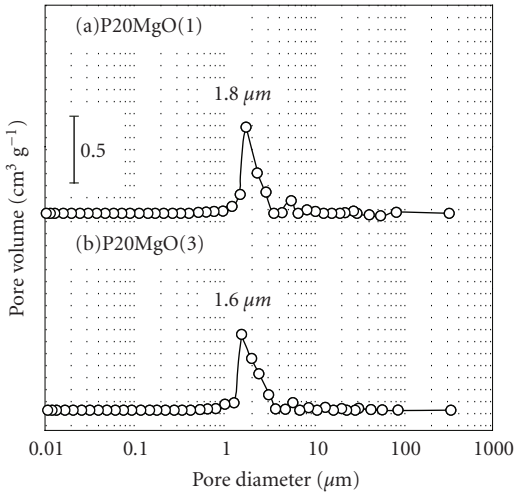

Figure 5: Pore size distributions of (a) P20MgO(1) and (b) P20MgO(3).

in P20NONE compact, and those in P20MgO(n) compact decreased with an increase in the amount of the MgO added, as summarized in Table 2. On the other hand, the crystallite size of P20MgO(n) compact increased with an increase in the amount of MgO added (see Table 2). These results show evidently that the addition of MgO promoted the sintering among α-Al_2O_3 grains and shrank both the PMMA-originated pores and the connected spaces.

Next, the effect of SiC addition on the microstructural morphology was examined to compare with that of MgO. SEM photographs and pore size distributions of P20SiC(n) compacts are shown in Figures 6 and 7. The diameters of both the PMMA-originated pores and the connected pores decreased with an increase in the amount of SiC added (see Table 2), as was observed in the case of the MgO addition. In addition, the crystallite size increased significantly from 20.9 nm for P20NONE compact to 42.8 nm for P20SiC(1) compact and 60.4 nm for P20SiC(3) compact. This means that the degree of sintering increased effectively by the addition of SiC rather than the addition of MgO. However, the pore volume and the open porosity increased greatly by the SiC addition (see Table 2), in contrast to the case of P20MgO(n) compacts. It is reasonable to consider that the added SiC will be subjected to oxidation during the sintering of the compacts, then resulted in the formation of SiO_2 and CO_2. And the resultant SiO_2 undoubtedly acts as a sintering aid. Thus, such preferable properties, that is, higher pore volume and open porosity, are considered to arise from the evolution of CO_2 gas during the oxidation of SiC added.

The addition of SiO_2 was also tested in order to clarify the role of SiC on the microstructural morphology of P20SiC(n) compacts. The XRD pattern, SEM photograph and pore size distribution of P20SiO_2(4.5) compact are shown in Figures 3(e), 6(c) and 7(c), respectively, and their microstructural data are also summarized in Table 2. No XRD peaks other than α-Al_2O_3 were observed and the crystallite size of α-Al_2O_3 for P20SiO_2(4.5) (57.4 nm) was comparable to that of α-Al_2O_3 for P20SiC(3) (60.4 nm). The average diameter of connected spaces in P20SiO_2(4.5) compact was slightly larger than that of P20SiC(3) compact. However, both the pore volume and the open porosity of P20SiO_2(4.5) compact became smaller than those observed for P20SiC(3) compact. These results confirm the excellent performance of SiC as a sintering aid to guarantee higher porous structure of the resultant ceramics and therefore the advantage of SiC in comparison with SiO_2.

3.2. Mechanical Properties of PmSA(n) Compacts. Figure 8 shows displacement-compressive stress curves of a series

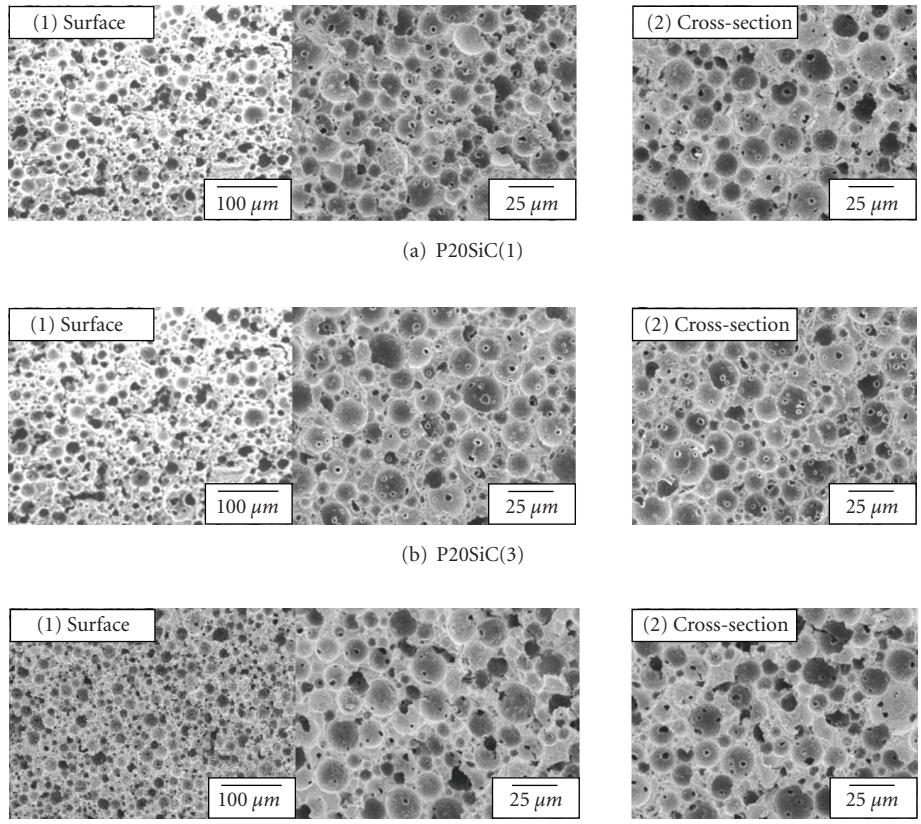

Figure 6: SEM photographs of (a) P20SiC(1), (b) P20SiC(3), and (c) P20SiO_2(4.5).

of P*m*NONE and representative P20SA(*n*) compacts. The compressive strength of each sample was calculated from the maximum of compressive stress, at which the sample was broken. The values of compressive strength of all compacts are listed in Table 2. The compressive strength of P*m*NONE compacts decreased drastically with an increase in the mean particle size of PMMA used, irrespective of almost the same pore volume as well as the same open porosity. Such a decrease in compressive strength may be ascribed to the increased diameter of the connected space and/or weaker ceramic walls forming PMMA-originated pores. The MgO addition resulted in an increase in the compressive strength, in comparison with those for P*m*NONE compacts, for example, 125.4 MPa for P20MgO(1) compact, 57.4 MPa for P60MgO(1) compact and 32.8 MPa for P90MgO(1) compact, due to the promotion of sintering. Furthermore, the addition of SiC seems to be more effective to improve the compressive strength than that of MgO, the compressive strength increased slightly from 138.5 MPa for P20MgO(3) compact to 147.6 MPa for P20SiC(3) compact. Variations in compressive strength of P20NONE and P20SA(*n*) compacts is plotted against the additive amounts of MgO or SiC, as shown in Figure 9. The compressive strength increased obviously with an increase in the additive amounts of the sintering aid for both MgO and SiC. Besides, the pore volume observed for P20SiC(3) compact was clearly larger than that for P20MgO(3) compact as summarized in Table 2, but the compressive strength of P20SiC(3) compact was slightly higher than that of P20MgO(3) compact. Therefore, the addition of an appropriate amount of SiC is considered to be superior to MgO as a sintering aid for porous α-Al_2O_3 compacts fabricated with PMMA microsphere as a template, that is, high open porosity consisting of well-developed and wide connected spaces among PMMA-originated pores and high compressive strength.

4. Conclusion

Highly porous alumina-based ceramics have been fabricated successfully by the slip casting method by employing PMMA microspheres as a template and MgO or SiC powder as a sintering aid and subsequent by sintering at 1600°C in air. In the case of P*m*SA(*n*) compacts, the resulting pores after removal of the PMMA microspheres were in an open pore of interconnected hollow microspheres whose porous shell walls consisted of α-Al_2O_3 particles. In this method, porous structure, for example, pore diameter, shape (open or closed) and mechanical properties, could be controlled by varying the particle size of PMMA microspheres and its concentration in alumina-based slurries. Compressive strength of P*m*SA(*n*) compacts increased with increasing the amount of MgO or SiC, while maintainig high open porosity,

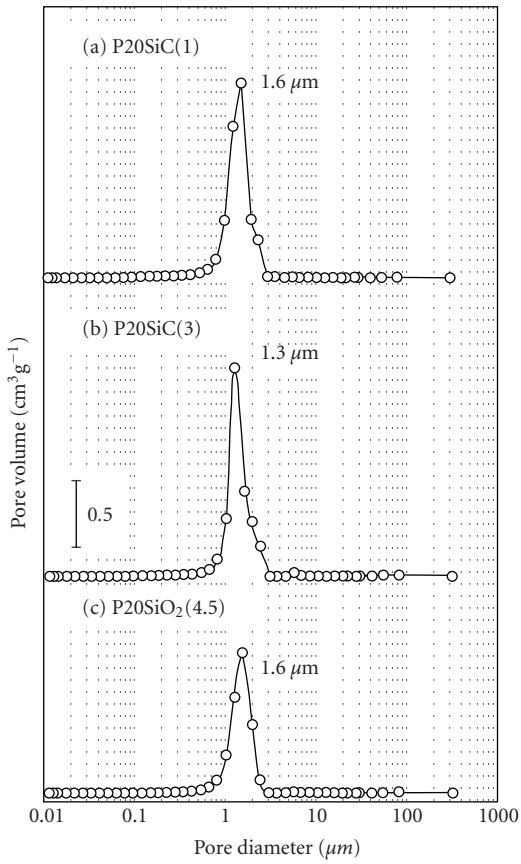

Figure 7: Pore size distributions of (a) P20SiC(1), (b) P20SiC(3) and (c) P20SiO_2(4.5).

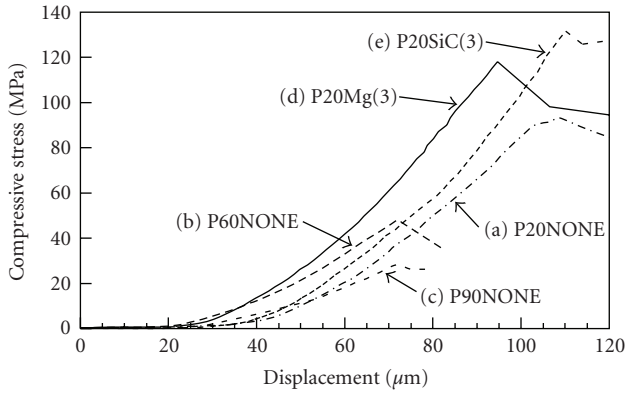

Figure 8: Variations in displacement-compressive stress curves of (a) P20NONE, (b) P60NONE, (c) P90NONE, (d) P20MgO(3), and (e) P20SiC(3).

but higher strength could be achieved with SiC. In addition, the advantage of SiC, in comparison with SiO_2, as a sintering aid to guarantee more porous structure could be confirmed. Among the porous compacts fabricated, P20SiC(3) had the most superior characteristics along with the open porosity of 62%, the connected space size of 1.3 μm, the compressive strength of 147.6 MPa.

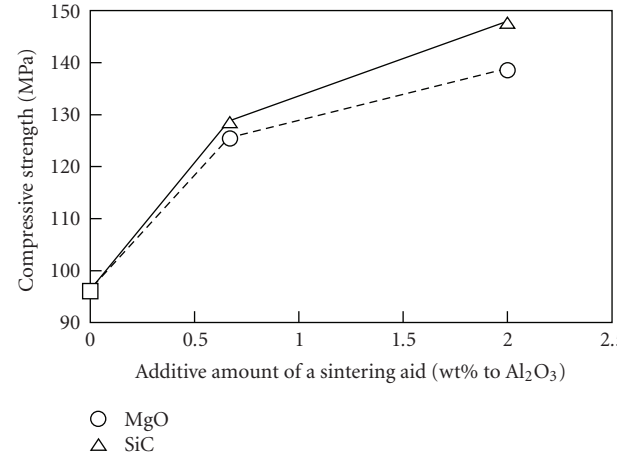

Figure 9: Variations in compressive strength of P*m*NONE and P*m*SA(*n*) compacts fabricated with MR-20G PMMA microspheres as a template as correlated with the additive amounts of MgO or SiC used as a sintering aid.

References

[1] F. Carn, A. Colin, M.-F. Achard, H. Deleuze, Z. Saadi, and R. Backov, "Rational design of macrocellular silica scaffolds obtained by a tunable sol-gel foaming process," *Advanced Materials*, vol. 16, no. 2, pp. 140–144, 2004.

[2] P. Sepulveda, "Gelcasting foams for porous ceramics," *American Ceramic Society Bulletin*, vol. 76, no. 10, pp. 61–65, 1997.

[3] P. Colombo and E. Bernardo, "Macro- and micro-cellular porous ceramics from preceramic polymers," *Composites Science and Technology*, vol. 63, no. 16, pp. 2353–2359, 2003.

[4] D.-M. Liu, "Preparation and characterisation of porous hydroxyapatite bioceramic via a slip-casting route," *Ceramics International*, vol. 24, no. 6, pp. 441–446, 1998.

[5] F. Mear, P. Yot, R. Viennois, and M. Ribes, "Mechanical behaviour and thermal and electrical properties of foam glass," *Ceramics International*, vol. 33, no. 4, pp. 543–550, 2007.

[6] C. Zou, W. Weng, X. Deng, et al., "Preparation and characterization of porous β-tricalcium phosphate/collagen composites with an integrated structure," *Biomaterials*, vol. 26, no. 26, pp. 5276–5284, 2005.

[7] A. Zampieri, P. Colombo, G. T. P. Mabande, T. Selvam, W. Schwieger, and F. Scheffler, "Zeolite coatings on microcellular ceramic foams: a novel route to microreactor and microseparator devices," *Advanced Materials*, vol. 16, no. 9-10, pp. 819–823, 2004.

[8] F. A. Costa Oliveira, "Elastic moduli of open-cell cordierite foams," *Journal of Non-Crystalline Solids*, vol. 351, no. 19-20, pp. 1623–1629, 2005.

[9] X. Mao, S. Wang, and S. Shimai, "Porous ceramics with trimodal pores prepared by foaming and starch consolidation," *Ceramics International*, vol. 34, no. 1, pp. 107–112, 2008.

[10] E. Saiz, L. Gremillard, G. Menendez, P. Miranda, K. Gryn, and A. P. Tomsia, "Preparation of porous hydroxyapatite scaffolds," *Materials Science and Engineering C*, vol. 27, no. 3, pp. 546–550, 2007.

[11] E. Bernardo, P. Colombo, and E. Manias, "SiOC glass modified by montmorillonite clay," *Ceramics International*, vol. 32, no. 6, pp. 679–686, 2006.

[12] K. Zhang, N. R. Washburn, and C. G. Simon Jr., "Cytotoxicity of three-dimensionally ordered macroporous sol-gel bioactive glass (3DOM-BG)," *Biomaterials*, vol. 26, no. 22, pp. 4532–4539, 2005.

[13] T. Kaito, A. Myoui, K. Takaoka, et al., "Potentiation of the activity of bone morphogenetic protein-2 in bone regeneration by a PLA-PEG/hydroxyapatite composite," *Biomaterials*, vol. 26, no. 1, pp. 73–79, 2005.

[14] X. Mao, S. Wang, and S. Shimai, "Porous ceramics with trimodal pores prepared by foaming and starch consolidation," *Ceramics International*, vol. 34, no. 1, pp. 107–112, 2008.

[15] S. J. Bryant, J. L. Cuy, K. D. Hauch, and B. D. Ratner, "Photo-patterning of porous hydrogels for tissue engineering," *Biomaterials*, vol. 28, no. 19, pp. 2978–2986, 2007.

[16] T. Isobe, Y. Kameshima, A. Nakajima, K. Okada, and Y. Hotta, "Gas permeability and mechanical properties of porous alumina ceramics with unidirectionally aligned pores," *Journal of the European Ceramic Society*, vol. 27, no. 1, pp. 53–59, 2007.

[17] J. R. Jones, L. M. Ehrenfried, and L. L. Hench, "Optimising bioactive glass scaffolds for bone tissue engineering," *Biomaterials*, vol. 27, no. 7, pp. 964–973, 2006.

[18] T. Tian, D. Jiang, J. Zhang, and Q. Lin, "Fabrication of bioactive composite by developing PLLA onto the framework of sintered HA scaffold," *Materials Science and Engineering C*, vol. 28, no. 1, pp. 51–56, 2008.

[19] T. Kato, H. Ushijima, M. Katsumata, T. Hyodo, Y. Shimizu, and M. Egashira, "Fabrication of hollow alumina microspheres via core/shell structure of polymethylmethacrylate/alumina prepared by mechanofusion," *Journal of Materials Science*, vol. 37, no. 11, pp. 2317–2321, 2002.

[20] K. Hieda, T. Hyodo, Y. Shimizu, and M. Egashira, "Preparation of porous tin dioxide powder by ultrasonic spray pyrolysis and their application to sensor materials," *Sensors and Actuators B*, vol. 133, no. 1, pp. 144–150, 2008.

[21] K. Sasahara, T. Hyodo, Y. Shimizu, and M. Egashira, "Macroporous and nanosized ceramic films prepared by modified sol-gel method with PMMA microsphere templates," *Journal of the European Ceramic Society*, vol. 24, no. 6, pp. 1961–1967, 2004.

[22] H. Seh, T. Hyodo, and H. L. Tuller, "Bulk acoustic wave resonator as a sensing platform for NOx at high temperatures," *Sensors and Actuators B*, vol. 108, no. 1-2, pp. 547–552, 2005.

[23] S. Nonaka, T. Hyodo, Y. Shimizu, and M. Egashira, "Preparation of macroporous semiconductor gas sensor and their odour sensing properties," *Chemical Sensors*, vol. 23, pp. 121–123, 2007.

[24] T. Kato, T. Hyodo, Y. Shimizu, and M. Egashira, "Aluminum-based composite with hollow alumina microspheres prepared by a mechanofusion method," in *Proceedings of the Annual Meeting of the Ceramic Society of Japan*, p. 97, Tokyo, Japan, May 2003.

[25] Y. Takakura, T. Hyodo, Y. Shimizu, and M. Egshira, "Preparation of macroporous Eu-doped oxide thick films and their application to gas sensor materials," *IEEJ Transactions on Sensors and Micromachines*, vol. 128, no. 4, pp. 137–140, 2008.

[26] Y. Sakka, A. Honda, T. S. Suzuki, and Y. Moriyoshi, "Fabrication of oriented β-alumina from porous bodies by slip casting in a high magnetic field," *Solid State Ionics*, vol. 172, no. 1–4, pp. 341–347, 2004.

[27] Y. Zhang, Y. Yokogawa, X. Feng, Y. Tao, and Y. Li, "Preparation and properties of bimodal porous apatite ceramics through slip casting using different hydroxyapatite powders," *Ceramics International*, vol. 36, no. 1, pp. 107–113, 2010.

[28] M. P. Albano, L. A. Genova, L. B. Garrido, and K. Plucknett, "Processing of porous yttria-stabilized zirconia by tape-casting," *Ceramics International*, vol. 34, no. 8, pp. 1983–1988, 2008.